

Interaction between aliasing and antialiasing effects in differentiating smooth band-unlimited signals

Vairis Shtrauss

Abstract—We study aliasing and antialiasing effects occurring in discrete-time differentiation of a smooth band-unlimited signal – so-called the Cauchy pulse through evaluation of differentiation errors for low frequency portion (LFP) below the Nyquist frequency and high frequency portion (HFP) above the Nyquist frequency produced by type IV linear phase differentiators designed by different methods with varying differentiators' lengths, sampling and band-limiting frequencies. We demonstrate that differentiation of HFP creates an *aliasing error* equal to the error of the computed HFP of the derivative, whereas removing HFP causes an algorithm-independent *antialiasing error* equal to HFP of the exact derivative with minus sign. Both errors are in a balance and determine the common error introduced by the band-unlimitedness. We disclose that regardless sampling frequency the antialiasing error in the differentiation is greater than the aliasing one. The differentiators designed by various methods approximately equally compute HFP with nearly equal aliasing errors having a weak dependence on differentiator length, at the same time, LFPs are differentiated with very wide variation in the accuracy. It is demonstrated that the differentiators with smooth magnitude responses at low frequencies compute considerably more accurate derivatives of LFPs than those having rippled responses.

Keywords—Aliasing and antialiasing errors, Cauchy pulse, Discrete-time differentiation, Smooth band-unlimited signals.

I. INTRODUCTION

THERE are branches of science and technology, such as material science [1], [2], mechanics [3], dielectric spectroscopy [4], geophysics [5], [6], etc. facing with measuring and processing monotonic signals, which can be generalized as smooth band-unlimited signals (BUSs). As it is well known [7]–[9], sampling a signal that is not band-limited produces aliasing distortions appearing as high frequency portion (HFP) of the signal above the Nyquist frequency generated back to the Nyquist frequency band.

In order to avoid the effect of aliasing, a common or even compulsory procedure is removing HFP by antialiasing filtering (AAF) prior to sampling [7]–[9] to make a BUS to be band-limited.

This work was supported by the European Regional Development Fund under project No. 1.1.1.1/16/A/008.

V. Shtrauss is with the Institute for Material Mechanics of the University of Latvia, 23 Aizkraukles Street, Riga, Latvia LV 1006 (phone: +371-67185363; fax: +371-67185362; e-mail: strauss@pmi.lv).

Despite that AAF more or less reduces the aliasing effect, i.e. prevents generating HFP back to the Nyquist frequency band, a new – antialiasing effect is produced by AAF due to loss of HFP with the appropriate antialiasing error, referred also to as frequency-truncation error [8] and cutoff error [10]. Both the effects influence the accuracy of discretely processed time domain waveforms of BUSs and a typical example is discretely computed derivatives [11].

At present, interaction between aliasing and antialiasing effects has not received much attention in the literature. The significance of the aliasing effect is often emphasized, but the antialiasing effect is typically ignored in processing of bandlimited signals assuming that it smaller than aliasing one [8]. Most of the work in discrete-time processing of BUSs is focused on sampling and reconstruction [12]–[15].

The goal of this study is to develop a more complete understanding of the interaction between the aliasing and antialiasing effects in discrete-time processing of time domain waveforms for BUSs and to give further insight into discrete-time differentiation to compute derivatives as accurately as possible. To achieve this goal, we evaluate errors of separate time-domain portions below and above the Nyquist frequency in differentiation of a smooth band-unlimited function (signal)

$$x(t) = 1/(1+t^2), \quad (1)$$

which sometimes is referred to as a Cauchy pulse [16].

The rest of this work is organized in three sections. In Section II, the background and evaluation methodology are described. The evaluation results are represented and analyzed in Section III. Section IV contains conclusions.

II. THEORETICAL BACKGROUND AND EVALUATION METHODOLOGY

A. Idea behind Research

The idea behind the research is to split the Cauchy pulse (1) into low frequency portion (LFP) below the Nyquist frequency and HFP above the Nyquist frequency, and evaluate differentiation errors of the derivatives for the full-band signal (1) and its portions produced by different discrete-time differentiators with varying the processing conditions. Block diagram in Fig. 1 illustrates the idea behind the research.

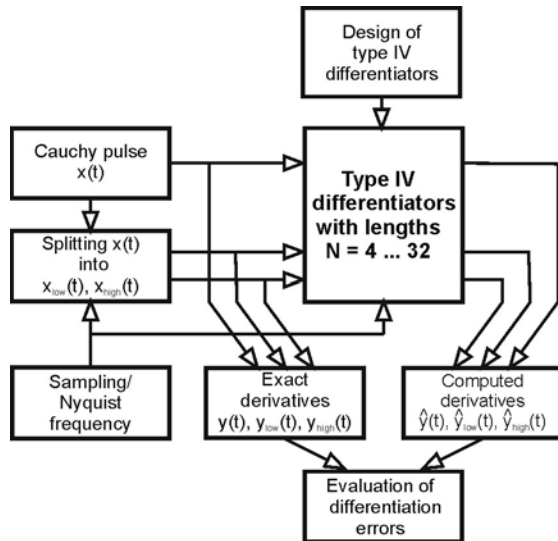


Fig 1 Block diagram of research of interaction between aliasing and antialiasing effects in differentiating BUS

B. Input and Output Signals

The band-unlimited input signal (1) – the Cauchy pulse increases monotonically in interval $t < 0$ and decreases monotonically in interval $t \geq 0$ (Fig. 2(a)). The choice of the Cauchy pulse was motivated by the fact that function (1) appears in several diverse applications, including material science [1] and [2], where the Cauchy pulse over the positive interval $[0, \infty)$ is widely used for modelling the real part of the complex permittivity and complex compliance.

According to the research idea (see Fig. 1), the Cauchy pulse (1) is split into LFP and HFP

$$x(t) = x_{low}(t) + x_{high}(t) \quad (2)$$

at the Nyquist frequency $\Omega_{Ny} = \Omega_s / 2$ as a splitting frequency, where Ω_s is angular sampling frequency.

The signal portions (2) are computed by taking the inverse Fourier transform of spectrum of the Cauchy pulse

$$X(\Omega) = \pi \exp(-|\Omega|)$$

over the frequency bands of interest. Such acquirement may be interpreted as determination of the portions by ideal filtering. Thus, LFP or band-limited version of (1) is determined as

$$x_{low}(t) = 1 / (2\pi) \int_{-\Omega_{Ny}}^{\Omega_{Ny}} X(\Omega) \exp(j\Omega t) d\Omega,$$

giving an expression

$$x_{low}(t) = x(t) [1 + \exp(-\Omega_{Ny}) (t \sin \Omega_{Ny} t - \cos \Omega_{Ny} t)]. \quad (3)$$

Computation of HFP may be simplified by calculation of a difference (see Fig. 2(b))

$$x_{high}(t) = x(t) - x_{low}(t). \quad (4)$$

Examples for waveforms of (3) and (4) are shown in Fig. 2(a) and Fig. 2(b) for the Nyquist frequency $\Omega_{Ny} = 2.5$.

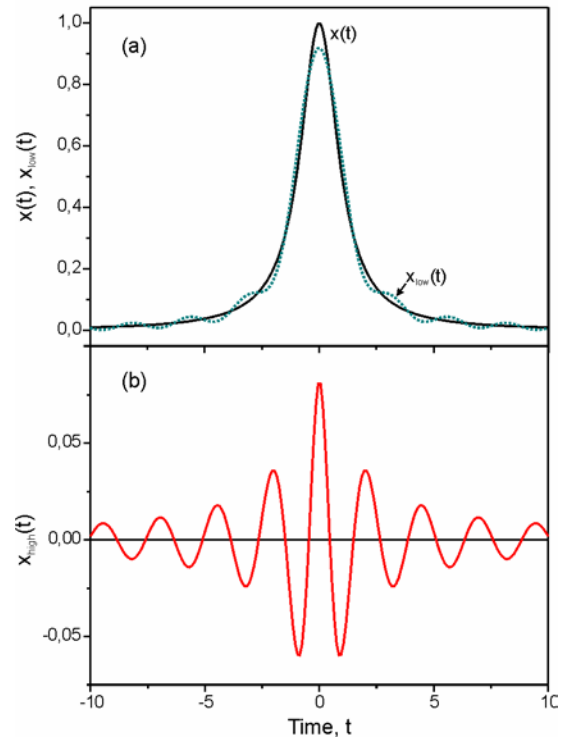


Fig. 2 The Cauchy pulse and its LFP (a) and HFP (b) split at the Nyquist frequency $\Omega_{Ny} = 2.5$

The Cauchy pulse and its LFP and HFP have the following derivatives (Fig. 3):

$$y(t) = x'(t) = -2tx^2(t), \quad (5)$$

$$y_{low}(t) = x'_{low}(t) = x^2(t) [-2t + 2t \exp(-\Omega_{Ny} t) \cos(\Omega_{Ny} t) - 2t^2 \exp(-\Omega_{Ny} t) \sin(\Omega_{Ny} t)] + x(t) \{ \exp(-\Omega_{Ny} t) [\Omega_{Ny} t \cos(\Omega_{Ny} t) + \sin(\Omega_{Ny} t) + \Omega_{Ny} \sin(\Omega_{Ny} t)] \}, \quad (6)$$

$$y_{high}(t) = x'_{high}(t) = y(t) - y_{low}(t). \quad (7)$$

From Figs. 2(a) and 3(a) is seen that due to the antialiasing errors, exact band-limited waveform $x_{low}(t)$ and its derivative $y_{low}(t)$, both having alias free discrete-time spectra identical with the continuous-time counterparts over the Nyquist frequency band, are distorted and deviate from the band-unlimited waveforms (1) and (5).

To acquire discrete-time versions, signals (1) and (3)-(7) are computed at the chosen Nyquist frequency Ω_{Ny} and sampled at the sampling frequency twice the Nyquist frequency $\Omega_s = 2\Omega_{Ny}$.

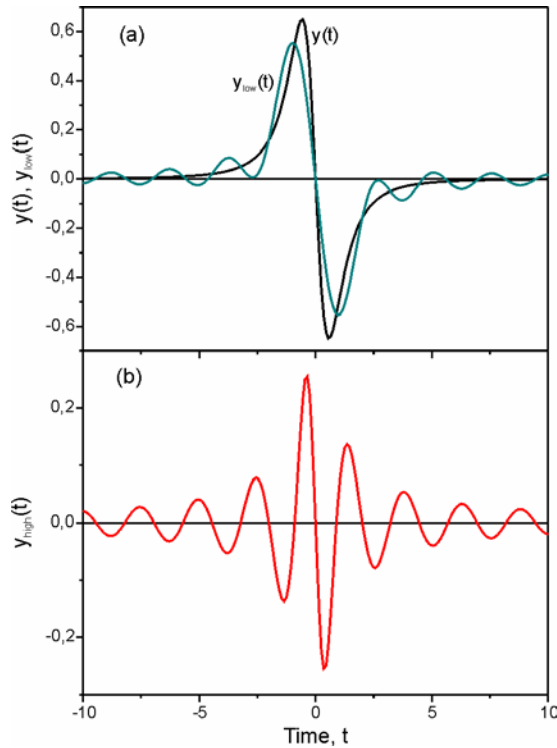


Fig. 3 Derivatives of the Cauchy pulse and its LFP (a) and HFP (b) split at the Nyquist frequency $\Omega_{Ny} = 2.5$

C. Evaluation of differentiation accuracy

Following the suggestion in [17], we define the accuracy of a derivative likewise to the measurement accuracy in the metrology [18] as closeness of agreement between a computed derivative and an exact derivative, where discrete-time versions of analytically derived derivatives (5)–(7) are used as exact ones. The accuracy of a computed derivative is estimated through a time-domain error determined as a difference between the computed signal $\hat{y}(t)$ and the exact one $y(t)$

$$e(t) = \hat{y}(t) - y(t), \quad (8)$$

which, in its turn, is evaluated by mean squared error (MSE), expressing the energy of error signal (8)

$$MSE = (1/M) \sum_{m=1}^M e^2(t_m) \quad (9)$$

In this study, MSE is calculated for fixed number of points ($M = 100$) over the predetermined time interval $[0, 10]$ of an output signal. MSE (9) is an accuracy criterion for both time domain waveforms, i.e. derivatives, and discrete-time algorithms, i.e. differentiators. The smaller MSE is, the more accurate the computed derivative and the differentiator are.

D. Time Domain Errors

According to (2), the common time domain differentiating error (8) is also composed from LFP and HFP components

$$e(t) = e_{low}(t) + e_{high}(t), \quad (10)$$

where

$$e_{low}(t) = \hat{y}_{low}(t) - y_{low}(t), \quad (11)$$

$$e_{high}(t) = \hat{y}_{high}(t) - y_{high}(t). \quad (12)$$

Error $e_{high}(t)$ establishes the error from non-bandlimitedness and, depending on processing conditions, constitutes both the aliasing and antialiasing errors. In the full-band processing mode without AAF, which can be identified as an extreme processing mode [11] with $\Omega_c = \infty$, it represents the maximum aliasing error with zero antialiasing error

$$e_{alias}(t) = \hat{y}_{high}(t) - y_{high}(t). \quad (13)$$

In the second extreme processing mode [11] with ideal AAF at $\Omega_c = \Omega_{Ny}$, HFP of the input signal is completely removed, i.e. $x_{high}(t) = 0$, resulting in $\hat{y}_{high}(t) = 0$ and $e_{high}(t) = -y_{high}(t)$. In this case, $e_{high}(t)$ describes the maximum antialiasing error with zero aliasing error at the given sampling/Nyquist frequency

$$e_{antialias}(t) = -y_{high}(t). \quad (14)$$

According to (10), the common differentiation error is constituted from the LFP error and error introduced by the band-unlimitedness, and is equal to

$$e_{full}(t) = e_{low}(t) + e_{alias}(t), \quad (15)$$

in the full-band processing mode, and

$$e_{AAF}(t) = e_{low}(t) + e_{antialias}(t) \quad (16)$$

in the processing mode with ideal AAF with cutoff at the Nyquist frequency.

Two important points follow from the above. First, it is revealed that the antialiasing error in the case of ideal AAF with cutoff at the Nyquist frequency is equal to HFP of exact derivative (7) with minus sign and, so, does not depend on the discrete-time algorithm used.

Second, it is easy to see from (13), that in the case when computed signal $\hat{y}_{high}(t)$ has the comparable amplitude and the same phase as those of exact signal $y_{high}(t)$, the signals $\hat{y}_{high}(t)$ and $y_{high}(t)$ will cancel each other, and the amplitude of aliasing error (13) will become smaller than the amplitude of antialiasing error (14). Therefore, depending on how input HFP generated back after sampling to the Nyquist frequency band is processed by the discrete-time algorithm used, both the aliasing and antialiasing error can predominate.

E. Discrete-Time Differentiators

We choose type IV linear phase differentiators with even number of coefficients [7]–[9] as promising the higher differentiating accuracy for band-unlimited applications compared with the type III differentiators. The differentiators were designed by several commonly known finite impulse response (FIR) filter design methods: the impulse response truncation (IRT) method [9], the Parks-McClellan (PM) algorithm [19], deriving by using maximal linearity (ML) constraints [20, 21], and identification (ID) method [2], [17].

IRT method was selected as the simplest and most straightforward FIR filter design method. It is usually mentioned in literature [9] as one generating filters with undesirable frequency-domain characteristics due to the oscillatory nature of the frequency response near cutoff frequencies, therefore, IRT filters may be conditionally classified as the “worst” ones for frequency selective filtering provided to modify the frequency content and phase of signals according to the definite specifications [7]–[9]. Contrary to IRT method, PM algorithm has been chosen as probably the most widely used FIR filter design method generating optimal filters in sense of minimax error with a minimum number of coefficients needed to achieve the given frequency domain specification [7]–[9]. Hence, PM filters may be conditionally categorized as the “best” ones frequency selective filters. Deriving by using ML constraints has been chosen as a favorable option [20, 21] preferable of filters for the applications, where the time domain properties are of primary importance.

To test the optimality of the differentiators designed by the methods mentioned above to compute the derivatives of BUSs as accurately as possible under the given processing conditions and to understand what might be the optimal algorithms for this purpose, the differentiators with the smallest attainable error were constructed also by ID method [2], [17] with minimizing MSE between the computed and exact derivatives in the full-band processing mode.

III. EVALUATION RESULTS AND DISCUSSION

A. Aliasing Error versus Antialiasing Error

One of the basic result of this study was a finding that the differentiation is the case, in which regardless sampling frequency the antialiasing error (14) is greater than the aliasing error (13).

In Fig. 4(a), as an example, HFP of derivative, computed by 12-point IRT differentiator at sampling frequency $\Omega_S = 5$, and exact HFP (7) are shown. It can be noticed, that signals $\hat{y}_{high}(t)$ and $\hat{y}_{high}(t)$ have the comparable amplitudes with the same phases, and, so, they cancel each other making that the amplitude of aliasing error (13) smaller the amplitude of antialiasing error (14) (see Fig. 4(b)).

Fig. 5 illustrates the behavior in the frequency domain, where the continuous-time magnitude spectrum $|Y_{high}(\Omega)|$ (colored) of exact HFP (7) is compared with the appropriate

discrete-time magnitude spectrum $|Y_{s,high}(\Omega)|$ of exact HFP (7) and spectrum $|\hat{Y}_{s,high}(\Omega)|$ of computed HFP at the same conditions as in Fig. 4.

According to (14), spectrum $|Y_{s,high}(\Omega)|$ constitutes the magnitude spectrum $|E_{antialias}(\Omega)|$ (Fig. 6) of antialiasing error, whereas the aliasing error, generated as difference (13), has magnitude spectrum $|E_{alias}(\Omega)|$. These spectra again confirm prevalence of antialiasing error over aliasing one.

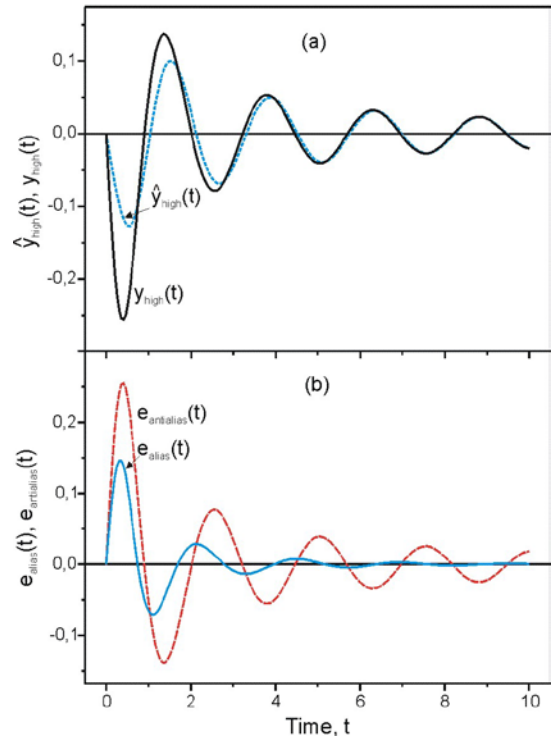


Fig. 4 Computed and exact HFP of the derivatives (a) and the appropriate aliasing and anti-aliasing errors (b) computed at sampling frequency $\Omega_S = 5$ by 12-point IRT differentiator

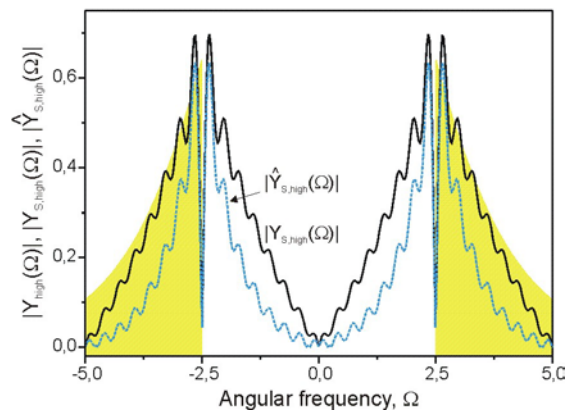


Fig. 5 Continuous-time spectrum (colored area) and discrete-time spectra of HFP of the derivative at $\Omega_{Ny} = 2.5$

A similarity between the spectra of aliasing and antialiasing errors is qualitatively kept regardless sampling/Nyquist frequency. For example, in Fig. 7, the spectra are shown for

the Nyquist frequency $\Omega_{Ny} = 10$. The discrete-time spectra in Figs. 5–7 are calculated by the discrete-time Fourier transform from the computed and exact derivatives over time intervals $[-40, 40]$.

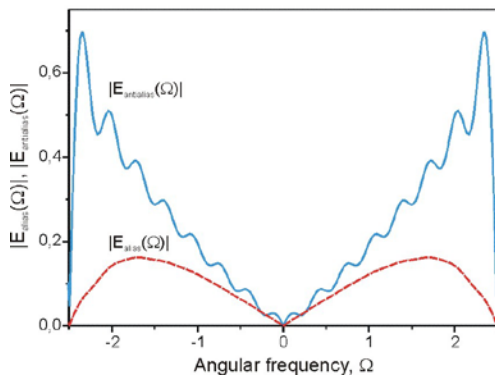


Fig. 6 Discrete-time magnitude spectra of the aliasing and anti-aliasing errors at $\Omega_{Ny} = 2.5$

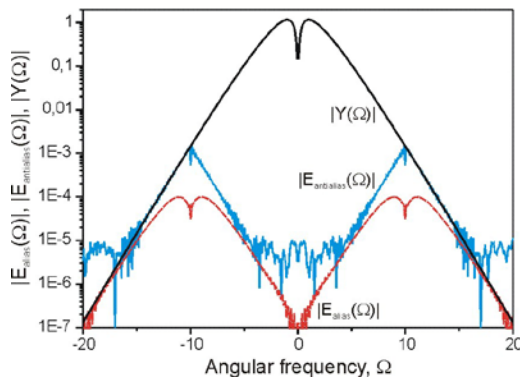


Fig. 7 Discrete-time magnitude spectra of aliasing and anti-aliasing errors at $\Omega_{Ny} = 10$ and continuous-time magnitude spectrum of the derivative of the Cauchy pulse (5)

B. Variation of Differentiation MSEs with Sampling Frequency

In Fig. 8(a), typical variation of differentiation MSEs with sampling frequency is shown for LFP, aliasing and anti-aliasing components, whereas MSEs of the derivatives in the full-band and AAF differentiation modes obtained for 12-point differentiators are presented in Fig. 8(b).

It is seen that anti-aliasing MSE is higher than aliasing one. Logarithmic plot of algorithm-independent anti-aliasing MSE is nearly straight line with negative slope meaning that $MSE_{antialias}$ decays almost exponentially with sampling frequency (and cutoff frequency in the case of ideal AAF).

The differentiators designed by different methods approximately equally process HFP producing nearly equal aliasing errors MSE_{alias} , which fall into the narrow lane (see Fig. 8(a)). ML and ID differentiators have practically undistinguishable aliasing errors that are slightly higher than those of PM and IRT differentiators, which also are basically undistinguishable. Logarithmic plots of the aliasing MSEs are straight with a narrow angle between the anti-aliasing MSE

witnessing that both MSEs are approximately proportional each other with a proportionality coefficient that slightly increases with growing sampling frequency.

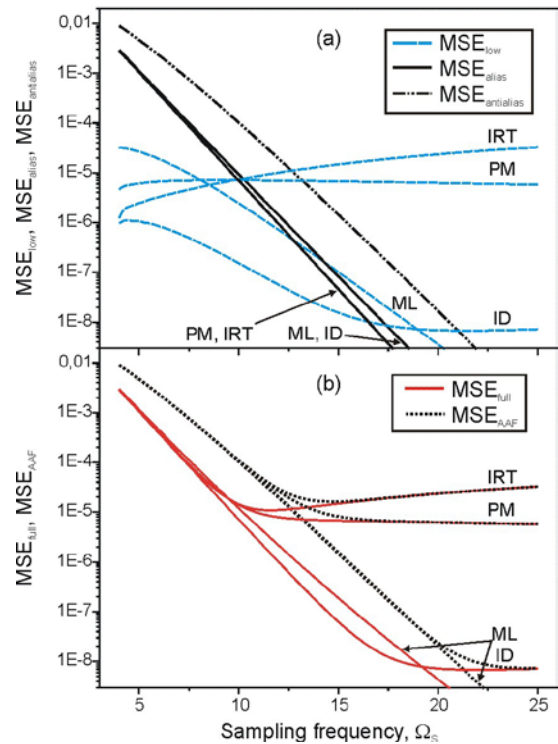


Fig. 8 Variation of differentiation MSEs with sampling frequency. LFP, aliasing and anti-aliasing MSEs (a). Complete MSEs in the full-band and AAF processing modes (b)

At the same time, LFP errors of differentiators designed by different methods behave very differently. For ML differentiator, MSE_{low} decreases almost exponentially (linearly on log–MSE scale), which together with the exponentially decaying aliasing and anti-aliasing errors constitute the common MSEs, which also have exponential nature. Consequently, increase of sampling frequency for ML differentiators leads to significant enhancement in the differentiation accuracy. ID method generates the most accurate differentiators, however, mainly in the vicinity of the sampling frequencies at which a differentiator is constructed. In Fig. 8, errors are shown for an ID differentiator designed at $\Omega_s = 14$.

In contrast to ML and ID differentiators, a little surprising result for us was slowly growing MSE_{low} for IRT differentiator and approximately constant MSE_{low} for PM differentiator (see Fig. 8(a)). Thus, improvement of the differentiation accuracy of these differentiators with increasing sampling frequency happen only at relatively low sampling frequencies thanks to decaying aliasing/anti-aliasing errors behaving in the approximately same way for all differentiators regardless design method (see Fig. 8(b)). Due to essentially lower LFP errors, ML and ID differentiators demonstrate essentially higher differentiation accuracy in both the full-band and AAF processing modes at higher sampling frequencies.

C. Variation of Differentiation MSEs with Differentiator Length

Typical variation of differentiation MSEs with differentiator length is shown in Fig. 9 for sampling frequency $\Omega_S = 14$. The plots of Fig. 9 afforce actually the results presented in the previous Subsection.

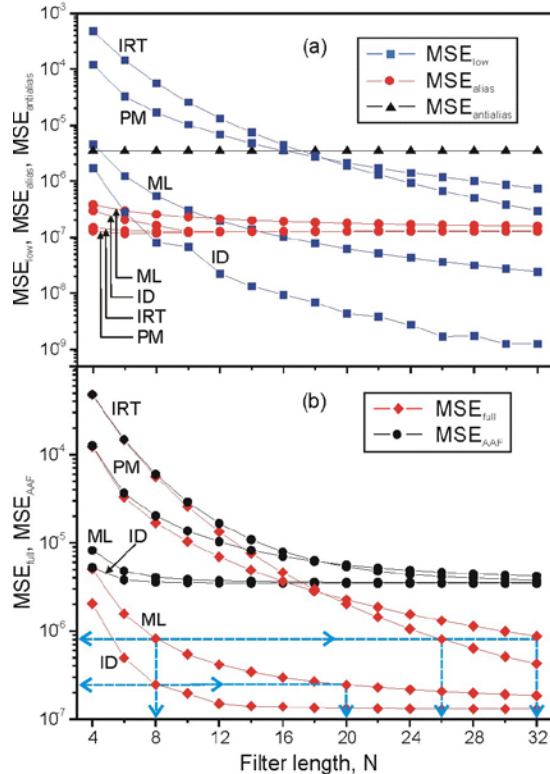


Fig. 9 Variation of differentiation MSEs with differentiator length. LFP, aliasing and anti-aliasing MSEs (a). Complete MSEs in the full-band and AAF processing modes (a)

It is seen again that the aliasing error is smaller than the antialiasing one. PM and IRT differentiators have practically equal aliasing error, whereas the aliasing error is slightly greater for ML and ID differentiators. The aliasing errors have a weak dependence on the differentiator length indicating on approximate proportionality with the antialiasing errors, particularly for the longer lengths.

Contrary to the aliasing errors, there are significant variation in MSEs of LFPs for differentiators designed by different methods. Again, ML differentiators produce much more accurate LFP derivatives compared to IRT and PM differentiators, however, ML differentiators do not reach the maximum possible accuracy achievable by ID differentiators.

As a result, ML and ID differentiators need a much smaller number of coefficients than PM and IRT differentiators to compute the derivatives of equal accuracy. For example, 8-point ID differentiator (see arrows in Fig. 9(b)) in the full-band processing mode has the same error ($MSE_{full} \approx 0.25 \cdot 10^{-6}$) as a 20-point ML differentiator. Extrapolation (not shown in Fig. 9(b)) indicates that IRT differentiator requires 36 coefficients, but PM differentiator – 48 coefficients to attain

this accuracy. Similarly, 8-point ML differentiator has the same error ($MSE_{full} \approx 0.82 \cdot 10^{-6}$) as 26-point IRT differentiator, and 32-point PM differentiator (coefficients are given in [19]).

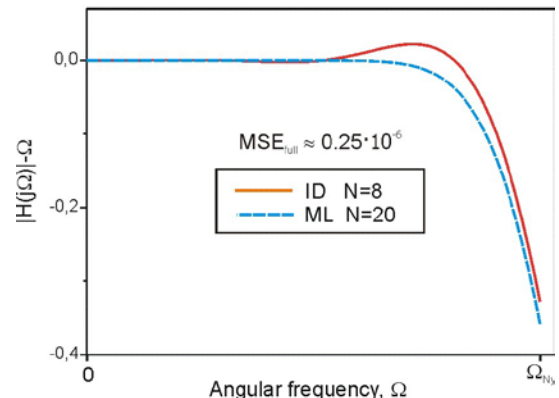


Fig. 10 Error responses for 8-point ID, and 20-point ML differentiators ensuring the same differentiation MSE in the full-band differentiating mode

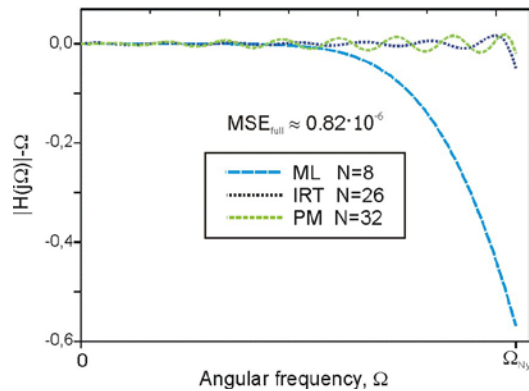


Fig. 11 Error responses for 8-point ML, 26-point IRT, and 32-point PM differentiators ensuring the same differentiation MSE in the full-band differentiating mode

Therefore, the conditionally “best” and “worst” differentiators according to the frequency selective filtering concept [7] – PM and IRT differentiators are not optimal in the sense of filter length criterion for computing accurate derivatives of LFPs. They are quite similar in differentiating accuracy for LFP that is much lower than that of ML differentiators and potentially maximally accurate ID differentiators.

In Fig. 10 and 11, deviations of magnitude responses from the true ones (error responses) $|H(j\Omega)| - \Omega$ are compared for some differentiators ensuring the equal accuracy in the full-band differentiating mode (indicated by arrows in Fig. 9(b)), designed by different methods with of various lengths.

It is seen that differentiators with smooth magnitude responses at low frequencies, such as ML and ID differentiators, are more preferable for attaining the derivatives of high accuracy for BUSs than those with well-fitted, but rippled magnitude responses, such as PM and IRT differentiators.

D. Variation of Aliasing and Antialiasing MSEs with Cutoff Frequency

In the previous Section, we demonstrate that error from the band-unlimitedness is limited by the maximum antialiasing error (14) corresponding to cutoff frequency $\Omega_c = \Omega_{Ny}$ and the maximum aliasing error (13) corresponding to $\Omega_c = \infty$. Within the frequency band $\Omega_{Ny} < \Omega_c < \infty$, both the antialiasing and aliasing errors exist together (Fig.12). The antialiasing error (14) exponentially decreases (see Fig. 8(a)) from a value at $\Omega_c = \Omega_{Ny}$ to zero at $\Omega_c = \infty$, whereas the aliasing error in the same time increases from zero to maximum one (13). So the errors neutralize each other and the common impact from the band-unlimitedness on the total differentiating accuracy is determined by a balance between the both errors: the more is suppressed the aliasing error, the more is magnified the antialiasing error, and vice versa. Since $MSE_{antialias} > MSE_{alias}$ in the differentiation, the balance error decreases with cutoff frequency.

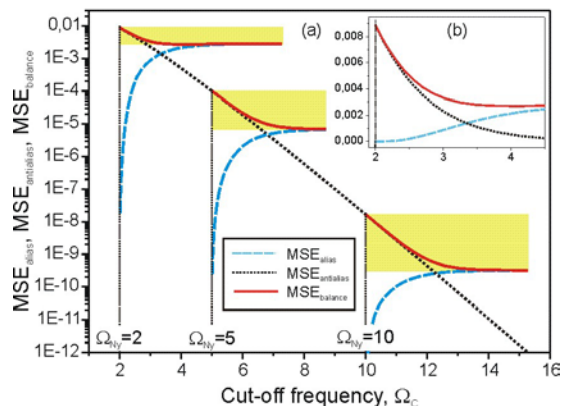


Fig. 12 Variation of aliasing, antialiasing and balance MSEs with cutoff frequency on logarithmic scale (a) and on linear scale (b).

Colored areas – intervals of variation of balance MSE

IV. CONCLUSIONS

We demonstrate that the band-unlimitedness influences the accuracy of discretely computed derivatives through: (i) an aliasing effect due to differentiating high frequency portion (HFP) above the Nyquist frequency generated back to the Nyquist frequency band by causing an aliasing error equal to the error of HFP of the derivative, and (ii) an antialiasing effect due to removing HFP creating an algorithm-independent antialiasing error equal to HFP of the exact derivative with minus sign. It is disclosed that regardless sampling frequency the antialiasing error in the differentiation is greater than the aliasing one. We find that type IV linear phase differentiators designed by various design methods, such as the impulse response truncation method, the Parks-McClellan algorithm, deriving by using maximal linearity constraints, and the identification method, approximately equally differentiate HFP and produce nearly equal aliasing errors having a weak dependence on the differentiators' lengths. At the same time, the mentioned differentiators very differently process low

frequency portion (LFP) below the Nyquist frequency, which limits the common differentiation accuracy. It is shown that differentiators with smooth magnitude responses at low frequencies, e.g. the differentiators derived by using maximal linearity constraints and constructed by the identification method, compute considerably more accurate LFPs than differentiators having rippled magnitude responses, e.g. the differentiators designed by the Parks-McClellan algorithm and the impulse response truncation method.

REFERENCES

- [1] N. G. McCrum, B. E. Read, and G. Williams, *Anelastic and Dielectric Effects in Polymer Solids*. London: J. Wiley and Sons, 1967.
- [2] V. Shtrauss, "Digital interconversion between linear rheologic and viscoelastic material functions," in: *Advances in Engineering Research*, vol. 3, V. M. Petrova, ed. New York: Nova Science Publishers, 2012, pp. 91–170.
- [3] J. D. Ferry, *Viscoelastic Properties of Polymers*. 3rd ed. New York: J. Wiley and Sons, 1980.
- [4] F. Kremer, A. Schonhals, and W. Luck, *Broadband Dielectric Spectroscopy*. Berlin: Springer-Verlag, 2003.
- [5] M. R. Gadallah, and R. Fisher, *Exploration Geophysics*. Berlin: Springer-Verlag, 2009.
- [6] P. Kearey, M. Brooks, and I. Hill, *An Introduction to Geophysical Exploration*. 3rd ed. Oxford: Blackwell Science, 2002.
- [7] A. V. Oppenheim, and R. V. Schaffer, *Discrete-Time Signal Processing*. New Jersey: Prentice-Hall, 1999.
- [8] S. M. Alessio, *Digital Signal Processing and Spectral Analysis for Scientists. Concepts and Applications*. Heidelberg: Springer Cham, 2016.
- [9] B. Porat, *A Course in Digital Signal Processing*. New York: J. Wiley and Sons, 1997.
- [10] E.-G. Woschni, "Errors with direct process -coupled digital sensors," in *Proc. 7th Int. Conf. Measurement*, Smolenice, Slovakia, 2009, pp. 3–6.
- [11] V. Shtrauss, "Time-domain aliasing and antialiasing effects in differentiating a band-unlimited signal," *MATEC Web Conf.*, vol. 210, 05005, 22nd International Conference on Circuits, Systems, Communications and Computers (CSCC 2018), Majorca, Spain, July 14-17, 2018.
- [12] P. P. Vaidyanathan, "Sampling Theorems for Nonbandlimited Signals," in *Sampling, Wavelets, and Tomography*, J. J. Benedetto, and A. I. Zayed, eds., Boston: Birkhauser, 2004, pp. 115-136.
- [13] S. Senay, L. F. Chaparro, and A. Akan, "Sampling and reconstruction of non-bandlimited signals using Slepian functions", in *16th European Signal Processing Conference (EUSIPCO 2008)*, Lousanne, Switzerland, August 25–29, 2008.
- [14] W. Sun, and X. Zhou, "The aliasing error in recovery of nonbandlimited signals by prefiltering and sampling," *Appl. Math. Lett.*, vol. 16, pp. 949–954, 2003.
- [15] A. Kumar, P. Ishwar, and K. Ramchandran, "Dithered A/D conversion of smooth non-bandlimited signals," *IEEE Trans. Signal Proc.*, vol. 58, no. 5, pp. 2654–2666, May 2010.
- [16] A. D. Poularikas, *Transforms and Applications Handbook*. 3rd ed. Boca Raton: CRC Press, 2010.
- [17] V. Shtrauss, "An approach to accurate inversion of convolution transforms by FIR filters," *WSEAS Trans. Signal Processing*, vol. 10, pp. 242 – 253, 2014.
- [18] *International Vocabulary of Metrology – Basic and General Concepts and Associated Terms (VIM)*, 3rd ed., JCGM 200:2012, 2012.
- [19] J. H. McClellan, T. W. Parks, and L. R. Rabiner, "A computer program for designing program for designing optimum FIR linear phase digital filters," *IEEE Trans. Audio Electroacoust.*, vol. AU-21, pp. 506–526, Dec. 1973.
- [20] I. R. Khan, and R. Ohba, "New design of full band differentiators based on Taylor series," *IEE Proc. – Vis. Image Signal Process.*, vol. 146, no.4, pp. 185–189, 1999.
- [21] I. R. Khan, M. Okuda, and R. Ohba, "Design of FIR digital differentiators using maximal linearity constraints," *IEICE Trans. Fundamentals*, vol. 87-A, no. 8, pp. 2010–2017, 2004.